

# Model for the density, temperature, and plasma potential of low-density hot-filament discharges

Scott Robertson and Zoltan Sternovsky

Department of Physics, University of Colorado, Boulder, Colorado 80309-0390, USA

(Received 6 December 2004; published 19 July 2005)

A theoretical model is developed for the density and temperature of confined electrons and the plasma potential in low-density hot-filament discharges. These three parameters are found from a simultaneous solution of the equations for ion particle balance, electron particle balance, and electron energy balance. In the model, electrons are lost by diffusion in velocity over the potential barrier determined by the plasma potential. The confined electrons are heated by the unconfined electrons that are the secondaries from the wall and, to a lesser extent, by the primary electrons from the filaments. The plasma parameters calculated from the model agree with parameters measured in a double plasma device that has been modified to have a clean wall that gives a single value for the confining potential.

DOI: [10.1103/PhysRevE.72.016402](https://doi.org/10.1103/PhysRevE.72.016402)

PACS number(s): 52.55.Dy

## I. INTRODUCTION

The electron temperature in nearly-collisionless hot-filament discharges, such as those in the double-plasma devices, is typically 0.1–5 eV. Although there has been considerable work on understanding particle and energy balance in these discharges, there is no widely accepted way to find the electron temperature from first principles. Many processes that can affect particle and energy balance have been found, including heating by secondary electrons from the walls and by primary electrons from the filaments [1–4]. These processes are also important for modeling ion sources [5,6] and ion thrusters [7]. The lack of a model for energy balance has considerable impact on the way in which experimental plasma physics is done. The experimentalist needing a nearly collisionless plasma with a particular density and electron temperature will typically go to the literature to find what device will give the desired plasma, rather than calculate what can be obtained with a given discharge current and filling pressure. In this work, a first-principles model is presented from which the plasma density, electron temperature and plasma potential can be calculated, for plasmas with a sufficiently low neutral density. The number density and energies of the energetic electrons that do the heating are required as inputs to the model. Experimental data are presented, which show that the model applies to an unmagnetized, hot-filament discharge in low-pressure gas ( $<1$  mTorr) with a plasma density in the range  $10^7$ – $10^8$   $\text{cm}^{-3}$ . The physical processes in the model have previously appeared in the literature. The model combines these known processes in a new way and finds the plasma parameters as simultaneous solutions to three equations. The model was developed for a double-plasma device [8] in which plasma is created by primary electrons from heated filaments. The plasma density in these devices can be increased by surface magnetic containment, [9,10] but the effects of these fields have not been included in the model.

In the model, the electrons are divided into the four populations illustrated in Fig. 1(a). Population I is the confined electrons that have energy less than  $qV_p$ , where  $q$  is the elementary charge and  $V_p$  is the plasma potential. The potential

difference  $V_p$  between the center of the plasma and the wall is assumed to occur primarily in a thin sheath at the wall that reflects the confined electrons. The wall potential is assumed to be zero. Population II is secondary electrons released from the wall by the primary electrons. These secondaries have a distribution that is approximately Maxwellian with a temperature of  $\sim 2$  eV. Population III is energetic primary electrons from the heated filaments that create the plasma by impact ionization of the neutral gas. These primaries are assumed to be monoenergetic with an energy determined by the difference between the filament bias potential and the plasma potential. The fourth population has its origin in the ionization of the neutral gas. Impact ionization creates secondary electrons with an energy distribution that has a width of approximately 10–15 eV, Fig. 1(b). Electrons created with energy less than  $qV_p$  become population I. The electrons created with energy greater than  $qV_p$  become population IV. For typical discharge conditions, populations II, III, and IV are a small fraction of the density. In 1925 Langmuir [11] showed by analysis of probe data that at least three populations (I, III, and IV) were present in hot-filament discharges in mer-

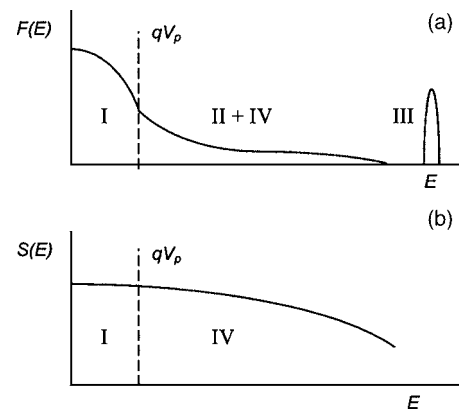


FIG. 1. (a) Plot of the electron energy distribution  $F(E)$  showing the locations of the four electron populations. (b) Plot of the source distribution  $S(E)$  of electrons created by impact ionization of the neutral gas. Electrons created with energy  $E$  below  $qV_p$  become population I electrons and those created with energy above  $qV_p$  become population IV.

cury. The division into populations with a dividing energy at  $qV_p$  was introduced into discharge modeling by Tsendin and Golubovskii [12].

The equation for ion particle balance, described in Sec. II A below, is easily written by balancing the rate of ionization with the rate of ion loss, which is calculable from the ion current density at the wall sheath. This current density is often attributed to Bohm [13] although the ion current in the collisionless sheath was first formulated by Tonks and Langmuir [14] and first solved in detail by Harrison and Thomson [15]. This collisionless sheath model was subsequently incorporated into “free fall” models of ion particle balance for the positive column [16,17] and into models for hot-filament discharges [2].

The input to the electron particle balance equation, in Sec. II B 1, is the rate of ionization. This work is focused on finding the parameters of the confined population, thus the source rate is the fraction of the ionization rate that corresponds to the creation of electrons with energy below  $qV_p$ . This fraction was introduced into discharge modeling by Brunet and Vincent [18]. It is this fraction of the ionization rate, which may be much smaller than one, that replenishes the confined electrons. In some models for the electron current to the walls, it is assumed that the electrons are Maxwellian and the loss current is then the random current of electrons reduced by the factor  $\exp(-qV_p/T_e)$ , where  $T_e$  is the temperature of the confined electrons in energy units. The walls of the device, however, are not a small perturbation and the distribution of confined electrons is depleted both at and above the energy  $qV_p$ . This depletion is easily observed in afterglows, [19] but is often not evident in active discharges because the distribution of confined electrons joins smoothly with the distribution of unconfined electrons.

Confined electrons diffuse in velocity and are lost at the boundary in velocity space that corresponds to the height of the potential barrier  $qV_p$ . Collisions with neutral atoms change the electron energy by a small fraction because of the small recoil of the more massive neutrals. At sufficiently low pressures, the electron velocity is changed primarily by collisions of confined electrons among themselves, which may be described by a transport equation with a Fokker-Planck collision operator, [20,21] discussed in Sec. II B 2. Loss by diffusion in velocity over the potential barrier has been modeled in detail for magnetic mirrors in which there is a strong ambipolar potential that confines the electrons [22–24]. For unmagnetized plasma, the loss boundary in velocity space can be modeled as a spherical surface and the solution for the loss rate can be obtained algebraically. The loss rate is a function of  $qV_p$ , thus  $qV_p$  may be determined as the potential that causes a loss of confined electrons that is equal to their rate of creation.

The rate of energy loss by confined electrons, Sec. II C 1, is simply the rate of particle loss multiplied by the energy  $qV_p$  that electrons carry when lost. Hershkowitz *et al.* [3] demonstrated experimentally that an important source of energy for the confined electrons is their equilibration with the more energetic unconfined electrons. This heating is incorporated into the model of energy balance, in Secs. II C 2 and II C 3, by finding the flow of energy from the unconfined populations to the confined population. The calculation is

made more accurate by finding the slowing of the populations of unconfined electrons using their distribution function, rather than by using a simpler equilibration time based upon two temperatures. In Sec. II C 4, the energy with which electrons are created is included as an additional energy source. The plasma potential is assumed to be below the first excitation potential, thus energy balance for the confined electrons is simplified because the confined electrons do not have these inelastic collisions.

Discharges in high-pressure gases (where the product of the radius and pressure is  $Pr > 50$  Torr cm) are collisional and thus are described by a fluid model in which the particle motion is from diffusion and mobility. Energy balance has been included in fluid models by finding higher order moments of the distribution function [25]. As the pressure is reduced ( $Pr < 1$  Torr cm), nonlocal kinetic models are used in which the distribution function is found from a two-term expansion of the Boltzmann equation [26,27]. Suprathermal electrons (with energy above the plasma potential) are lost preferentially, a process called diffusive cooling [28]. This cooling has been included in “zero-dimensional” kinetic models by having a cutoff in energy [29] and has been included in greater detail by making the electron distribution a function of both radius and velocity with transport by diffusion and mobility in the radial direction [30–36]. In these models, electrons are driven to higher velocity by the dc electric field. Particles with energy above the plasma potential have diffusive motion toward the wall, in contrast to the model presented here in which this loss is immediate. Electron-electron collisions described by a Fokker-Planck collision operator have been included in several models of low-pressure discharges (negative glows, [37] afterglows, [38] RF, [39] and microwave discharges [40]). The model presented here, which considers only electron-electron collisions, is most like the model of Arslanbekov and Kudryavtsev [37] that also includes electron-atom collisions that result in electron and ion losses being diffusive rather than “free flight.” There have been several reviews of discharge models for plasmas sufficiently collisional for the losses to be described by diffusion and mobility [23,41,42].

In Sec. III, data from a modified double plasma device are presented which support the model. The calculated plasma potential and electron temperature are within about 20% of model values over about an order of magnitude in density. Agreement between the model and the data required inserting clean metal liners into the experiment in order to have a more uniform wall potential. The modifications to the experiment are described in detail because the model will fail if applied to an experiment with “dirty” walls. Data are presented to illustrate the changes observed in the probe data when the walls are sufficiently clean to provide a uniform wall potential. The model is used to find additional plasma parameters such as the mean particle lifetime and equilibration times in Sec. IV and these parameters are used to examine the validity of the assumptions. In Sec. V is a conclusion.

## II. PHYSICAL MODEL

The model requires three equations to find the variables  $n_e$ ,  $T_e$  and  $V_p$ , where  $n_e$  is the density of confined electrons.

The first equation is the ion particle balance equation, which gives a relation between density and temperature of confined electrons. The second and third equations are for electron particle balance and electron energy balance.

### A. Ion particle balance

Ion particle balance is particularly simple because the ion current density at the wall has approximately the Bohm saturation value  $\sim 0.5 n_0 q c_s$ , where  $n_0$  is the ion density,  $q$  is the elementary charge,  $c_s = \sqrt{T_e/m_i}$  is the ion sound speed and  $m_i$  is the ion mass. Because of the quasineutrality requirement,  $n_0$  is also the sum of the densities of the four populations of electrons. This relation with a numerical coefficient 0.5 applies for collisionless planar discharges having dimensions of  $>10^3$  Debye lengths and can be found from the sheath model initially developed by Tonks and Langmuir [14]. A homogeneous ionization source function is appropriate for discharges in which the ionization is by energetic electrons that have few collisions before hitting the wall. For homogeneous ionization and cylindrical geometry, Self [43] and Self and Ewald [44] found from both a kinetic and a fluid model a coefficient of 0.42. In a recent paper, Sternovsky [45] investigated the effect of ion-neutral collisions on the ion flux to the wall in cylindrical geometry. The collisionless coefficient 0.42 is reduced due to charge-exchange collisions by approximately 8%, when the radius of the plasma is one mean free path. The reduction is by 20% when the radius is three mean free paths. In this work, the cylindrical value of 0.42 is used for the coefficient and the small ( $\sim 10\%$ ) collisional correction is ignored.

The ion particle balance equation is obtained by setting the creation rate of ions equal to the integrated flux of ions to the walls. For homogeneous ionization, the number of ions created per unit time is  $RV$ , where  $R$  is the ionization rate and  $V$  is the plasma volume. The number of ions lost per unit time is the product of the ion flux and the area  $A$  of the wall. The ion particle balance equation is then

$$RV = 0.42A n_0 \sqrt{T_e/m_i}. \quad (1)$$

The mean ion lifetime  $\tau_{ion}$  is

$$\tau_{ion} = \frac{n_0}{R} = \frac{2.4V}{A\sqrt{T_e/m_i}} = \frac{1.2r^*}{\sqrt{T_e/m_i}}, \quad (2)$$

where we have defined  $r^* = 2V/A$  as the approximate radius for a cylindrical plasma. This may be rearranged to express the density as a function of the electron temperature and the ionization rate

$$n_0(T_e) = \frac{1.2r^*R}{\sqrt{T_e/m_i}}. \quad (3a)$$

Alternatively, this equation can be written

$$R(n_0, T_e) = \frac{n_0 \sqrt{T_e/m_i}}{1.2r^*}, \quad (3b)$$

which treats the ionization rate as the dependent variable.

## B. Electron particle balance

### 1. Source rate for confined electrons

The confined electrons are replenished by the fraction of electrons from ionization with energy below the confining potential  $qV_p$ . The distribution of secondaries from ionization found by Opal *et al.*, [46] is approximately

$$S(E) = \frac{2}{\pi W} \left( \frac{1}{1 + (E/W)^2} \right), \quad (4)$$

where the distribution has been normalized to unity,  $E$  is the energy of the secondary electron,  $W=10$  eV for Ar, and  $W=15.8$  eV for He. The validity of this expression for  $E < 1$  V is discussed in Ref. [47]. This distribution was measured for primary electron energies large in comparison with the ionization energy [46]. For primary energies that are smaller, this distribution is a poor approximation because the true distribution is cut off at the energy of the incident electron minus the ionization energy. The fraction  $F(V_p)$  of secondary electrons that is confined by the plasma potential is [18,48]

$$\begin{aligned} F(V_p) &= \frac{\int_0^{qV_p} \frac{dE}{1 + (E/W)^2}}{\int_0^P \frac{dE}{1 + (E/W)^2}} \\ &= \frac{\arctan(qV_p/W)}{\arctan(P/W)} \cong \frac{qV_p}{W \arctan(P/W)}, \end{aligned} \quad (5)$$

where  $P = q(V_p - V_{fil}) - I$ ,  $P$  is the maximum energy of a secondary electron from ionization,  $V_{fil}$  is the filament bias potential, and  $I$  is the energy to ionize the neutral. The rate of replacement of confined electrons is  $F(V_p)R$  and the mean electron lifetime  $\tau_{elec}$  is

$$\tau_{elec} = \frac{n_e}{F(V_p)R} = \frac{1.2r^*}{F(V_p)\sqrt{T_e/m_i}}. \quad (6)$$

The flux to the wall of confined electrons is  $F(V_p)RV$  and the flux to the wall of secondaries from ionization that are not confined is  $[1 - F(V_p)]RV$ . The sum of these particle fluxes is equal to the ion flux  $RV$ . Although impact ionization creates electrons and ions at the same rate, the confined electrons are replaced at a lower rate than the ions and thus have a longer mean lifetime.

### 2. Electron particle balance

In a steady state, the rate of generation of confined electrons is balanced by their loss through diffusion in velocity over the confining potential barrier. This diffusion is described by the Fokker-Planck equation with a source term, [49]

$$\begin{aligned} \frac{\partial f}{\partial t} &= \frac{1}{v^2} \frac{\partial}{\partial v} \left\{ YI(x) \left[ f(v) + \frac{v}{2x^2} \frac{\partial f(v)}{\partial v} \right] \right\} + S(v) \\ &= -\frac{1}{v^2} \frac{\partial}{\partial v} [v^2 \Gamma(v)] + S(v), \end{aligned} \quad (7)$$

where

$$I(x) = n_f \left[ \Phi(x) - x \frac{d\Phi}{dx} \right], \quad (8)$$

$v$  is the radial electron velocity in spherical coordinates,  $f(v)$  is the distribution of confined electrons,  $S(v)$  is the source distribution function,  $Y = 4\pi(q^2/4\pi\epsilon_0 m_e)^2 \ln \Lambda$ ,  $4\pi v^2 \Gamma(v)$  is the flux of particles through a spherical surface at velocity  $v$ ,  $\Phi(x) = \text{erf}(x)$ ,  $x^2 = m_e v^2 / 2T_f$ ,  $n_f$  is the number density of field particles,  $T_f$  is the temperature of the field particles, the expression for  $I(x)$  is for field particles that are Maxwellian, and  $\ln \Lambda$  is the Coulomb logarithm. For a Maxwellian distribution colliding with itself,  $n_f = n_e$ ,  $T_f = T_e$ , the two terms in the curly brackets are equal and opposite, and the distribution does not change if  $S(v) = 0$ . In a steady state, the integral of  $4\pi v^2 S(v) dv$  is the ionization rate  $R$ . The rate of loss of electrons by diffusion over the barrier is  $4\pi v^2 \Gamma(v)$  evaluated at the velocity  $w = \sqrt{2qV_p/m_e}$  corresponding to the height of the barrier.

In a steady state, the flux of electrons through a spherical surface in velocity space at radius  $v$  is equal to the rate of production of electrons with velocity less than  $v$ . Thus the particle balance equation for trapped electrons is obtained by setting the ionization rate for the trapped fraction equal to the loss by diffusion at the velocity  $w$ . We multiply Eq. (7) by  $4\pi v^2$  and integrate once to obtain

$$4\pi v^2 \Gamma(v) = F \left( \frac{1}{2} m v^2 \right) R, \quad (9)$$

thus

$$F \left( \frac{1}{2} m v^2 \right) R = -4\pi Y I(x) \left[ f(v) + \frac{T_e}{m_e v} \frac{\partial f}{\partial v} \right]. \quad (10)$$

We assume that the distribution function can be written  $f(v) = f_0(v) + f_1(v)$  where  $f_0(v)$  is a Maxwellian. We find for  $v^2 \gg 2T_e/m_e$

$$f_1(v) \cong - \frac{RF \left( \frac{1}{2} m v^2 \right)}{4\pi Y I(x)}, \quad (11)$$

where we have used that the term with  $\partial f_1 / \partial v$  is negligible for  $v^2 \gg 2T_e/m_e$ , which can be verified *a posteriori*. The total distribution of confined electrons,  $f_0(v) + f_1(v)$ , descends to the phase space density of the population II electrons [see Fig. 1(a)] at the velocity  $w$  corresponding to the energy  $qV_p$ , or

$$\begin{aligned} f(w) &= n_e \left[ \frac{m_e}{2\pi T_e} \right]^{3/2} \exp[-qV_p/T_e] - \left( \frac{RF(qV_p)}{4\pi Y I(\sqrt{qV_p/T_e})} \right) \\ &= n_{se} \left( \frac{m_e}{2\pi T_{se}} \right)^{3/2} \approx 0. \end{aligned} \quad (12)$$

For the conditions of our experiment, the phase space density of secondaries is negligible in comparison with the other terms in the equation and can be set equal to zero. From this approximation and Eq. (6), we obtain

$$qV_p/T_e = - \ln \left( \frac{RF(V_p)[2\pi T_e/m_e]^{3/2}}{4\pi Y n_e^2} \right) = \ln[4\pi v_{ee} \tau_{elec}], \quad (13)$$

where we have used that  $I(x) \rightarrow n_e$  for suprathermal velocities and have defined a collision frequency  $v_{ee} = n_e Y (m_e/2\pi T_e)^{3/2}$  that is approximately the Spitzer electron-electron collision frequency. This shows that the dimensionless parameter  $qV_p/T_e$  is approximately 7 when the electron lifetime is about 100 electron-electron collision times. An analogous expression for collisional plasma has been derived by Arslanbekov and Kudryavtsev [37] who set equal the losses of ions by spatial diffusion and the losses of confined electrons by diffusion in velocity.

## C. Electron energy balance

### 1. Energy carried by lost electrons

Confined plasma electrons are lost to the wall if  $v \cos \theta > \sqrt{2qV_p/m_e}$  where  $v \cos \theta$  is the component of velocity perpendicular to the wall [12]. We assume that the angular scattering is sufficiently rapid that electrons are lost soon after the energy  $qV_p$  is passed and that the energy at the time of loss is  $qV_p$ . The rate of energy loss per confined electron is then  $qV_p / \tau_{elec}$ .

### 2. Electron heating by primaries

The heating of the confined electrons by energetic primaries is calculated most easily by finding the energy lost by the primaries. For primaries with velocity  $v_{pri}$  and with energy  $U_{pri} = 0.5 m_e v_{pri}^2$  that is much greater than the energy of the confined electrons, the energy loss rate per primary electron is [49]

$$\frac{dU_{pri}}{dt} = \frac{-Y n_e m_e}{v_{pri}}. \quad (14)$$

An equilibration time  $\tau_{pri}$  can be defined using

$$\frac{1}{\tau_{pri}} = \frac{-1}{U_{pri}} \frac{dU_{pri}}{dt} = \frac{2Y n_e}{v_{pri}^3}. \quad (15)$$

The rate of energy gain per confined electron is then

$$\frac{dQ}{dt} = - \frac{n_{pri}}{n_e} \frac{dU}{dt} = \frac{n_{pri}}{n_e} \frac{U_{pri}}{\tau_{pri}}, \quad (16)$$

where  $Q$  is the energy transferred to a confined electron. The mean energy gained by a confined electron is obtained by multiplying this transfer rate by the mean lifetime  $\tau_{elec}$ .

### 3. Electron heating by wall secondaries

Langmuir probe traces from devices often show a high temperature tail that is secondary electrons from the wall. Wall secondaries have a characteristic energy of  $\sim 2$  eV that is nearly independent of the primary energy and of the wall material [50,51]. The wall secondaries are accelerated into the plasma by the sheath at the wall and are likely to be absorbed at the wall after one transit. Their mean lifetime in

the plasma is so short that they are not significantly heated or cooled by collisions with the confined electrons. The confined electrons, however, have a much longer mean lifetime and may be heated significantly by the wall secondaries. This heating can be the dominant source term in the energy balance equation for the confined electrons.

For an observer on the axis of the discharge, all electrons with kinetic energy below  $qV_p$  are confined electrons, and all electrons with energy above  $qV_p$  are primaries, wall secondaries, or secondaries from ionization. The confined electrons occupy a region in velocity space that is not shared with the other populations. The wall secondaries, when observed near the center of the discharge, have a distribution function that is hollow in velocity space. At the energy  $qV_p$ , the distribution function of confined electrons should join smoothly with the distribution of unconfined electrons as a consequence of diffusion in velocity across the boundary at  $qV_p$ , as illustrated in Fig. 1(a).

The heating by the wall secondaries can be found from Eq. (14) by treating the wall secondaries as an ensemble of beams. The loss by the ensemble is

$$\begin{aligned} n_{se} \frac{dQ_{se}}{dt} &= -Y n_e m_e \left\langle \frac{n_{se}}{v} \right\rangle \\ &= -Y n_e m_e n_{se} \left( \frac{m_e}{2\pi T_{se}} \right)^{3/2} \exp(qV_p/T_{se}) \\ &\quad \times \int_w^\infty \exp(-m_e v^2/2T_{se}) 4\pi v dv, \\ &= \frac{-2m_e Y n_e n_{se}}{v_{t,se} \sqrt{\pi}}, \end{aligned} \quad (17)$$

where  $v_{t,se} = \sqrt{2T_{se}/m_e}$  is the thermal velocity of the wall secondaries,  $T_{se}$  is the temperature of the wall secondaries, and the angled brackets denote an average over the distribution function of wall secondaries. The acceleration of the wall secondaries by the sheath at the wall results in the minimum velocity of secondaries being  $w = \sqrt{2qV_p/m_e}$ . Note that the energy transfer rate is independent of  $V_p$  as a result of cancellation of exponential factors. An equilibration time  $\tau_{se}$  can be defined for the secondaries by

$$\frac{1}{\tau_{se}} = -\frac{1}{T_{se}} \frac{dQ_{se}}{dt} = \frac{4Y n_e}{v_{t,se}^3 \sqrt{\pi}}, \quad (18)$$

and the rate at which energy is transferred to a confined electron is then

$$\frac{dQ_{se}}{dt} = \frac{n_{se} T_{se}}{n_e \tau_{se}}. \quad (19)$$

The integral in Eq. (17) is written in spherical coordinates using the assumption that the distribution function of wall secondaries is spherically symmetric. In our experiments, the secondaries originate from both the cylindrical walls and the end walls, thus the geometry is neither purely cylindrical nor spherical. Spherical geometry is used because in our experiment the area of the end caps is not a negligible fraction of the chamber surface area.

#### 4. Mean energy of electrons from ionization

The energy distribution of electrons from ionization, Eq. (4) and Fig. 1(b), is nearly flat for energies much less than  $W$ , thus for  $qV_p \ll W$  the mean energy of electrons born confined is  $0.5 qV_p$ . We neglect the electrostatic potential energy of electrons at their place of birth. This requires that the sheath at the wall occupy a negligible fraction of the plasma volume. The potential well of the presheath is approximately parabolic and has a depth of order  $T_e$ . For  $T_e \ll qV_p$ , the correction for the nonzero potential energy in the presheath is a small fraction of  $qV_p$ .

#### 5. Effects of collisions with neutrals

Collisions of electrons with neutrals results in energy loss as a consequence of recoil by the neutrals. This loss rate is approximately  $\frac{3}{2} T_e (2m_e/M) \nu_m$  where  $M$  is the mass of the neutrals and  $\nu_m$  is the electron-neutral collision frequency for momentum transfer. The rate of energy loss per confined electron can be written  $-\frac{3}{2} T_e / \tau_n$  where  $\tau_n = M / (2m_e \nu_m)$  is the characteristic energy loss time. The collision frequency  $\nu_m$  can be found from the momentum-transfer collision cross section, which for 1 eV electrons colliding with argon is of order  $10^{-16} \text{ cm}^2$ . For the conditions of our experiment, the calculated energy loss rate is very much less than the heating rate from wall secondaries and thus can be ignored.

Another mechanism for electron loss is collisions with metastable neutral atoms causing a deexcitation that gives sufficient energy to the electron for it to be lost over the potential barrier. In the inverse of this process, an unconfined electron loses energy and becomes confined. A calculation of the populations of metastable atoms is beyond the scope of this work. The fact that the plasma parameters from the model are near to those measured in the experiment suggests that metastable atoms are not important for energy balance at the low pressures ( $< 1 \text{ mTorr}$ ) employed in our experiment.

#### 6. Energy balance

The energy balance equation is obtained by summing the gains and losses to obtain

$$\frac{1}{2} \frac{qV_p}{\tau_{elec}} + \frac{n_{pri}}{n_e} \frac{U}{\tau_{pri}} + \frac{n_{se} T_{se}}{n_e \tau_{se}} - \frac{qV_p}{\tau_{elec}} - \frac{\frac{3}{2} T_e}{\tau_n} = 0, \quad (20)$$

where the terms in the equation correspond to the mean energy at birth, the energy transferred from primaries, the energy transferred from wall secondaries, the energy carried to the wall by electrons that are lost, and the energy lost in electron-neutral collisions. We assume that cooling by collisions with neutrals and heating by primaries are negligible and find

$$qV_p = 2T_{se} \frac{n_{se} \tau_{elec}}{n_e \tau_{se}}. \quad (21)$$

This may be combined with Eqs. (5) and (6) for electron particle balance to obtain

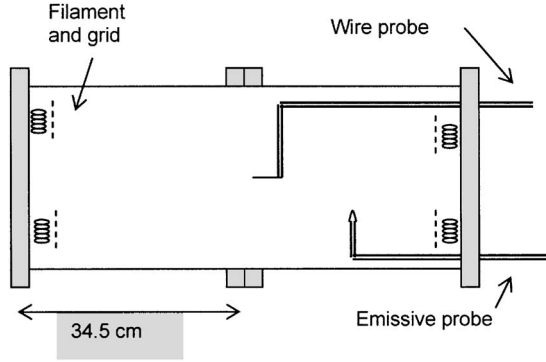


FIG. 2. The experimental apparatus.

$$qV_p(T_e, n_{se}, T_{se}) = \left[ \frac{2.4r^*W \arctan(P/W) \left( \frac{n_{se}T_{se}}{n_e\tau_{se}} \right)}{\sqrt{T_e/m_i}} \right]^{1/2}. \quad (22)$$

The product  $n_e\tau_{se}$  is independent of  $n_e$ , thus the function  $V_p(T_e, n_{se}, T_{se})$  has no explicit dependence upon  $n_e$  or  $R$ .

The model equations are solved in the following way. In Eq. (13),  $qV_p$  is replaced using Eq. (22) and  $n_e$  is replaced using Eq. (3a) by using that the confined electron density is approximately equal to the total electron density,  $n_e \cong n_0$ . The result is a transcendental equation with  $T_e$  as the unknown and with independent variables  $r^*$ ,  $n_{se}$ , and  $T_{se}$ :

$$G(T_e, n_e) = \frac{qV_p(T_e, n_{se}, T_{se})}{T_e} + \ln \left( \frac{R(n_e, T_e) F(V_p(T_e, n_{se}, T_{se})) [2\pi T_e/m_e]^{3/2}}{4\pi Y n_e^2} \right) = 0. \quad (23)$$

The roots of the function  $G(T_e, n_e)$  provide  $T_e$  as a function of  $n_e$ . It is then possible to make plots of  $T_e$ ,  $qV_p(T_e, n_{se}, T_{se})$  and  $R(n_e, T_e)$  as a function of  $n_e$ . Alternatively, Eq. (3b) may be used in place of Eq. (3a) and  $n_e$ ,  $T_e$ , and  $V_p$  may be found as a function of  $R$ . The variable  $n_{se}$  requires knowledge of experimental conditions thus the model is not entirely self-contained.

### III. EXPERIMENTS

#### A. Vacuum chamber

The experiments are performed in an aluminum cylindrical chamber 30 cm in diameter and 69 cm in length, Fig. 2. Two filaments 3 cm long are located on each of the two end flanges. Grounded stainless steel meshes are placed immediately above the filaments. The filament bias potential is  $-70$  V and the total emission current is 20–160 mA. A turbomolecular pump creates the vacuum and plasmas are generated in 0.2–0.8 mTorr of argon. The plasma parameters are determined by a cylindrical Langmuir probe of stainless steel wire (radius  $95 \mu\text{m}$  and length 27 mm) located on the axis. Before measurements are made, the probe is cleaned by heating to incandescence through applying large positive bias

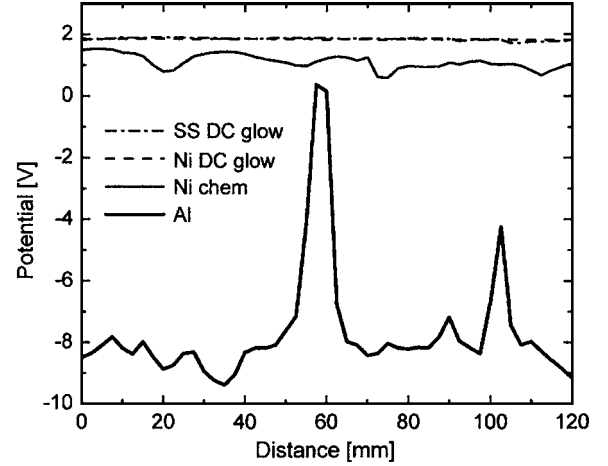


FIG. 3. The potential adjacent to the wall determined using the emissive probe. The data are for discharges in the aluminum chamber and in the chamber with nickel and stainless steel liners cleaned by a dc glow discharge. Also shown is the potential for the nickel liner cleaned by using chemical solvents prior to the application of the dc glow. The emissive data have a positive offset of approximately 1.5 V relative to ground.

potential. An emissive probe [52] is used to monitor the radial potential distribution, the plasma potential on the axis, and the potential very near the chamber walls. The emissive probe is a small semicircular loop (2 mm in diameter) of  $50 \mu\text{m}$  diameter tungsten wire on a movable shaft. The emissive probe readings provide only a relative measure of the plasma potential because of contact potentials and the voltage drop across the filament.

It is known from previous experiments in our device that the properties of the chamber walls facing the plasma have a large effect on probe data [53] and on plasma confinement [54]. An emissive probe was scanned axially along the wall of the aluminum chamber in typical discharge conditions. The separation between the probe filament and the wall, approximately 1 mm, was kept constant. The potential just above the aluminum surface was found to have spatial variations of almost 10 V due to uneven contamination, Fig. 3. The lack of a clearly defined wall potential blurs the boundary between confined and unconfined electrons. In order to provide a single-valued wall potential, liners of thin sheet metal were inserted to cover the walls. One liner is of stainless steel and the other is of nickel. Nickel was chosen because it does not form an oxide layer. The end flanges were covered with the same material as the liners and a stainless steel mesh was installed over the pumping port. An insertable anode was used occasionally to discharge clean the liners which improves the uniformity of the wall potential [54]. After these efforts, a sharp increase in the probe current was observed at a probe potential near zero volts, which indicated the boundary between the confined and unconfined electrons [53].

#### B. Langmuir probe interpretation

The Langmuir probe data are analyzed using orbit-motion-limited (OML) theory for cylindrical probes [55,56].

For a Maxwellian population of electrons, the probe current is given by

$$I_e(\eta) = 2\pi a L J_e \exp(\eta), \quad \eta \leq 0,$$

$$I_e(\eta) \cong 2\pi a L J_e \sqrt{1 + \frac{4\eta}{\pi}}, \quad \eta > 0, \quad (24)$$

where  $J_e = n_e q \sqrt{T_e / 2\pi m_e}$  is the random current of confined electrons,  $\eta = q(V_b - V_p) / T_e$ ,  $V_b$  is the probe bias potential,  $a$  is the probe radius, and  $L$  is the probe length. The density of a population is evaluated using the saturation current, which is defined as the current measured at  $\eta = 0$ . The derivative of the probe current has a maximum at  $\eta = 0$  which provides the method for determining the plasma potential.

For probe potentials more negative than the wall potential, no confined electrons are collected and thus the probe current is from primaries, wall secondaries and secondaries from ionization. In our device, the largest of these currents is the current of wall secondaries and these are assumed to be Maxwellian. For this population, the OML formulas are used with  $\eta = qV_b / T_{se}$ , where  $V_p$  is set to zero because the secondaries originate at the wall potential, which is very nearly zero when the walls are clean. For the wall secondaries,  $J_e$  is replaced by  $J_{se} = n_{se} q \sqrt{T_{se} / 2\pi m_e}$ , which is the random current of wall secondaries. At probe voltages more positive than the wall potential, the current from the secondaries is in the saturation regime.

The ion contribution to the probe current is also found from OML theory using the limit of small temperature. Laser-induced fluorescence measurements have shown that the temperature of ions in hot-filament discharges is close to room temperature, i.e.,  $T_i \approx 0.025$  eV [57,58]. The ion current thus can be assumed absent for bias potentials more positive than the plasma potential. From OML theory, Eq. (24), the current scales approximately with the square root of the potential for negative bias. There is an additional contribution to the probe current from ion-neutral collisions occurring near the probe [59–61]. It has been shown that this current scales approximately linearly with bias potential, thus an appropriate function for fitting these two ion currents is

$$I_i(V_b) = A \sqrt{-(V_b - V_p)} + B(V_b - V_p), \quad V_b \leq V_p, \quad (25)$$

where  $A$  and  $B$  are constants to be determined.

The probe data are analyzed by the method described in detail in Ref. [53]. First, the current of ions fitted in the

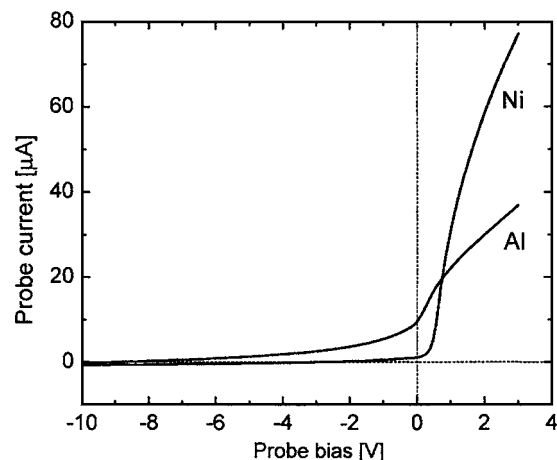


FIG. 4. Plot of Langmuir probe current as a function of bias voltage for a discharge with the contaminated aluminum walls (Al) and with the nickel liner (Ni).

region from approximately  $-10$  to  $-40$  V is subtracted from the total current. Second, the OML theory is fitted to the current of secondary electrons from a point near  $-6$  V to the wall potential  $V_{wall}$ . The wall potential is determined by a fitting routine that finds the voltage at which the slope of a logarithmic plot of probe current changes from  $T_{se}$  to  $T_e$ . Third, the current of wall secondaries is extrapolated to positive voltages using Eq. (24) for  $\eta > 0$  and this extrapolated current is subtracted from the total current at positive voltages to obtain the current from confined electrons alone. The OML theory is fit to this current from  $V_{wall}$  to approximately  $+3$  volts to find  $n_e$  and  $T_e$ .

### C. Effect of wall surface materials on plasma parameters

Figure 4 shows the remarkable difference between the raw Langmuir probe data without a liner and with a clean Ni metal liner. The traces shown are both for an emission current of 80 mA and a gas pressure of 0.39 m Torr. All other discharge conditions are identical. The discharges with the liners have a much lower density of secondaries from the wall. The floating potential  $V_{float}$  of the probe (see Table I) occurs at a negative voltage for which no confined electrons are collected. Thus the floating potential is determined by the balance of ion current with the currents of electrons from the unconfined populations. There is a higher density of wall

TABLE I. Plasma parameters for both the secondary and confined electrons deduced from the Langmuir probe data for 80 mA filament emission and 0.39 mTorr gas pressure. The wall potential,  $V_{wall}$ , for discharges with metal liners is determined from the break in the slope of the probe data. For discharges in aluminum, the wall potential is determined by varying the discharge pressure, as in Fig. 5. Data marked with an asterisk are very approximate because the distribution of secondaries originates at multiple wall potentials.

|                 | $T_{se}$ (eV) | $n_{se}$ (cm <sup>-3</sup> ) | $T_e$ (eV) | $n_e$ (cm <sup>-3</sup> ) | $V_{float}$ (V) | $V_{wall}$ (V) |
|-----------------|---------------|------------------------------|------------|---------------------------|-----------------|----------------|
| Stainless steel | 2.44          | $0.8 \times 10^6$            | 0.08       | $9.7 \times 10^7$         | -2.3            | 0              |
| Nickel          | 2.35          | $1.5 \times 10^6$            | 0.16       | $9.8 \times 10^7$         | -3.7            | -0.1           |
| Aluminum        | 3.50*         | $8.9 \times 10^6$ *          | 0.33       | $2.5 \times 10^7$         | -9.2            | -1.3           |

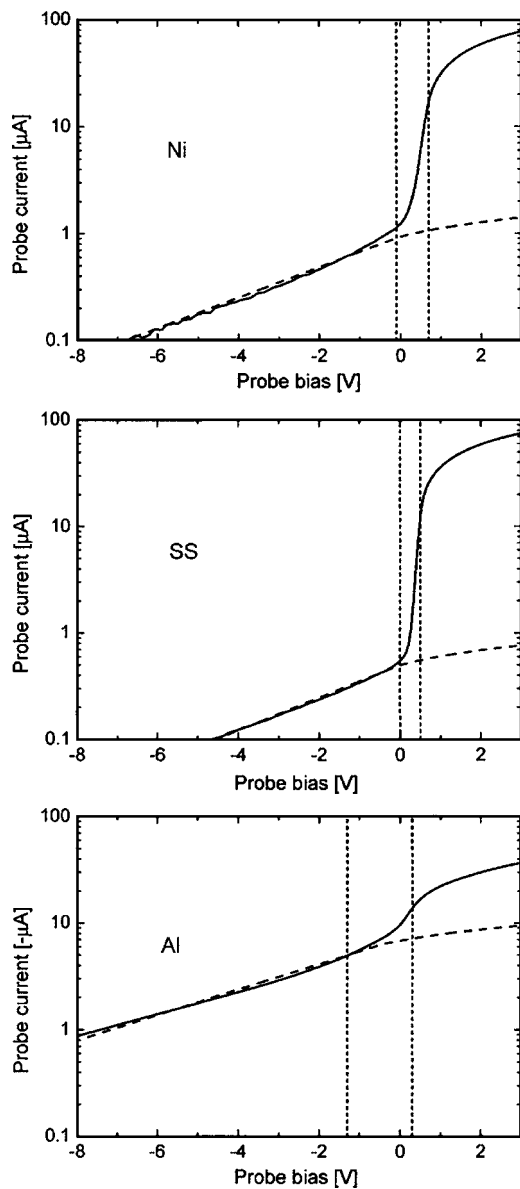


FIG. 5. Probe current, after subtracting the ion contribution, for the nickel liner, the stainless steel liner, and the contaminated aluminum. The vertical line at or to the left of zero marks the deduced wall potential  $V_{wall}$  and the vertical line to the right of zero marks the deduced plasma potential  $V_p$ . The dotted line is the fitted current for the unconfined electrons.

secondaries in the discharge without the liners and this results in a more negative floating potential.

Figure 5 shows the electron probe current for the same discharge conditions with a stainless steel liner, a nickel liner, and contaminated aluminum. The plotted data have the fitted ion current subtracted so that only the electron current is displayed. The measurements with the liners show clearly that the electron current increases sharply when the probe potential passes near zero. This increase is the onset of the collection of confined electrons. For all discharges with liners, the wall potential determined from the change in slope is within 0.2 V of zero, which supports the interpretation that this point is the onset of collection of confined electrons. To

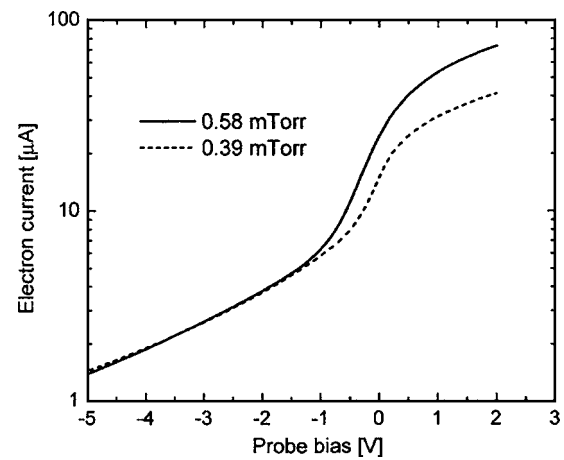


FIG. 6. Langmuir probe data for two pressures in the aluminum chamber without a liner. The current from the confined electrons is increased at the higher pressure and the current of wall secondaries is not changed. The data show that the confined electrons are collected for voltages more positive than about  $-1.3$  V.

the left of the wall potential, the probe plots for the liners have a slope corresponding to a temperature of  $\sim 2.4$  eV. This is approximately the temperature expected for secondary electrons emitted from metals. The deduced wall potentials and the plasma parameters for the wall secondaries are listed in Table I.

The discharges with the aluminum wall cannot easily be decomposed into currents from wall secondaries and from confined electrons. The probe data, Fig. 5, do not show the abrupt change in slope that would allow a precise determination of the wall potential. The break is obscured because of the larger fraction of secondary electrons, the higher temperature of confined electrons, and because the potential of the wall regions from which secondary electrons originate is multi-valued. Large regions are at approximately the floating potential (Fig. 3) indicating that these regions are poorly conducting. The confined electrons are lost at the most positive regions. These regions define an effective wall potential and an effective wall area for electron loss that is much less than the total area. The majority of secondary electrons are likely to originate from places several volts more negative than the effective wall potential and these electrons gain several electron volts of energy when accelerated through the sheath at the wall. These higher energy electrons add to the probe current when it is more positive than about  $-8$  V and give a false appearance of a higher “temperature” for the secondary electrons (observable in Fig. 5). The fitted “temperature” for these electrons is 3.5 eV, which is significantly higher than the  $\sim 2$  eV expected for clean metals.

An estimate of the effective wall potential for the discharges in aluminum can be found by varying the pressure while keeping the filament emission current constant. This procedure gives discharges in which the number of confined electrons is changed with a negligible change in the properties of wall secondaries. These probe data, Fig. 6, show that the current from the confined electrons rises above the current of wall secondaries at potentials more positive than approximately  $-1.3$  V. This effective value for the wall poten-



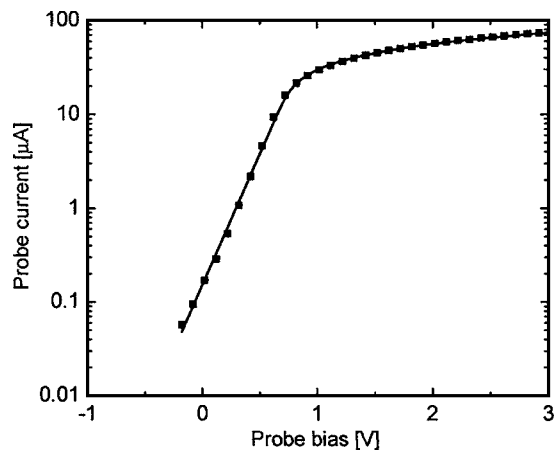


FIG. 7. Langmuir probe current corrected for the contribution of ions and wall secondaries. This current is from the confined electrons alone. The data are the points (separated by 0.1 V) and the fitted OML theory is the line. The exponential part of the curve has a nearly constant slope (corresponding to 0.155 eV) for more than 5  $e$ -foldings.

tial is used in the analysis of the probe data for unlined aluminum that appears in Table I.

The current from confined electrons alone for the case of the nickel liner is shown in Fig. 7. This plot is made by subtracting from the probe data the extrapolated current of wall secondaries. The current is very nearly exponential for more than 5  $e$ -foldings and is fit well by OML theory at both retarding and accelerating probe voltages. For the aluminum wall, the model that is used to subtract the current of wall secondaries is not accurate because the secondaries originate at different wall potentials. The current deduced for the confined electrons is thus less accurate and is not well fit by OML theory. For this reason the plasma parameters deduced for the unlined aluminum chamber (Table I) are also less accurate.

The temperature of the confined electrons is 0.08 eV for the stainless steel liner, which generates the lowest density secondary electrons, and is 0.33 eV with the bare aluminum the walls which generates a much higher number density of secondaries. These data show clearly that the temperature of the confined electrons is closely associated with the number density of wall secondaries.

TABLE II. Comparison of measured parameters with calculated parameters from the model. The first column is the discharge current and the next three columns are measured parameters that are inputs to the model. The data are for the Ni liner and 0.39 mTorr argon. Columns 5 and 6 are the measured and calculated electron temperatures for the confined electrons and columns 7 and 8 are the measured and calculated plasma potentials.

| $I_{dis}$ (mA) | Inputs to model                  |               |                               | $T_e$<br>meas. (eV) | $T_e$<br>calc. (eV) | $V_p$<br>meas. (V) | $V_p$<br>calc. (V) |
|----------------|----------------------------------|---------------|-------------------------------|---------------------|---------------------|--------------------|--------------------|
|                | $n_{se}(10^{12} \text{ m}^{-3})$ | $T_{se}$ (eV) | $n_e(10^{12} \text{ m}^{-3})$ |                     |                     |                    |                    |
| 20             | 0.46                             | 2.0           | 36                            | 0.09                | 0.07                | 0.51               | 0.52               |
| 40             | 0.82                             | 2.0           | 62                            | 0.11                | 0.09                | 0.66               | 0.65               |
| 80             | 1.52                             | 2.3           | 98                            | 0.16                | 0.12                | 0.88               | 0.80               |
| 120            | 2.33                             | 2.3           | 138                           | 0.18                | 0.14                | 1.03               | 0.94               |
| 160            | 2.94                             | 2.2           | 164                           | 0.19                | 0.16                | 1.10               | 1.03               |

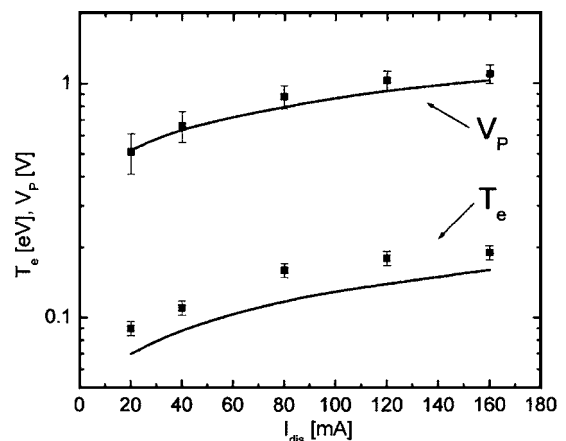


FIG. 8. The measured plasma potential  $V_p$  and the temperature of confined electrons  $T_e$  are plotted as a function of the discharge current  $I_{dis}$ . The uncertainty in the  $V_p$  determination (measured relative to  $V_{wall}$ ) is approximately 0.1 V. The error bars on the temperature are determined by making repeated sweeps at constant conditions. The solid lines are from the model with the measured  $n_{se}$ ,  $T_{se}$ , and  $n_e$  as input parameters.

#### D. Comparison of experiments with the model

The model was tested by applying it to two series of discharges, one with different discharge currents and the other with different gas pressures. The nickel liner was used rather than the stainless steel liner in order to have higher electron temperatures that improved the accuracy of the probe analysis. In the first parameter scan, the discharge current was varied from 20 mA to 160 mA and the pressure was held constant at 0.39 mTorr. The density of wall secondaries and the ionization rate  $R$  both increase with increasing discharge current, thus two input parameters of the model,  $n_{se}$  and  $R$ , were varied. The measured density and temperature of wall secondaries, and the measured density of confined electrons were used as inputs to the model. The confined electron density is used as the independent variable as an alternative to the ionization rate  $R$  that is not measured directly. The output parameters of the model are the temperature of the confined electrons and the plasma potential. The output parameters are compared with the measured values in Table II and Fig. 8. The discharge current is changed by a factor of eight and the

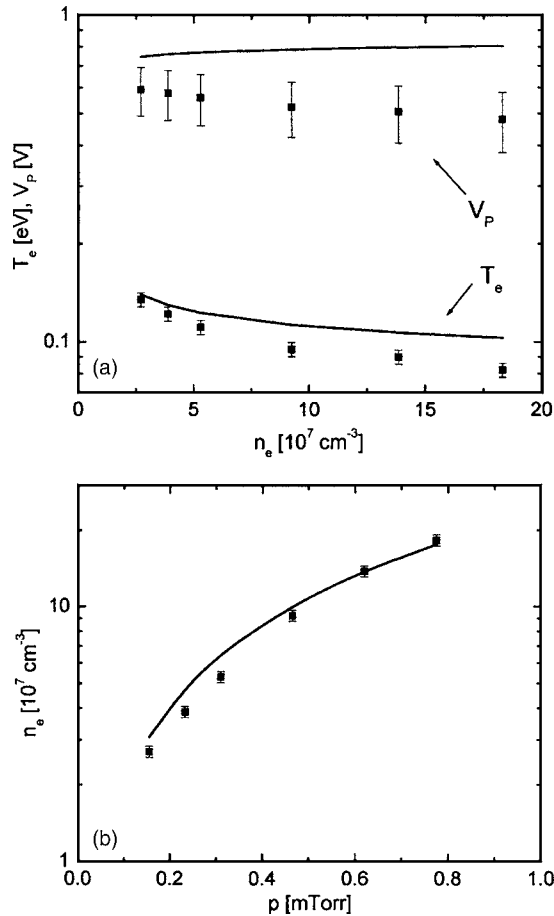


FIG. 9. (a) The plasma potential  $V_p$  and the temperature of confined electrons  $T_e$  are plotted as function of the measured plasma density  $n_e$ . The data were taken by varying the gas density from 0.16 to 0.8 mTorr with constant 80 mA emission. (b) The confined electron density is plotted as a function of the pressure. The input parameters to the model are  $n_{se}$  and  $T_{se}$  (approximately constant) and the ionization rate  $R$  is calculated from the pressure and emission current. The error bars on the density are determined by making repeated sweeps at constant conditions.

density by nearly a factor of five. For this range of conditions, the model values for  $T_e$  and  $V_p$  follow the measured values to within about 20%.

In the second parameter scan, Fig. 9, the filament emission is held constant at 80 mA and the pressure is varied from 0.16 to 0.8 mTorr. This procedure changes the ionization rate  $R$  and has negligible effect on the density of wall secondaries. This scan has the advantage of changing only one input parameter,  $R$ ; however, there is the disadvantage that Eq. (22) for energy balance does not contain  $R$  and thus the dependence of  $T_e$  upon  $R$  is weak. The plot in Fig. 9(a) shows that the model values for electron temperature are slightly higher than the measured values with the level of error increasing to  $\sim 20\%$  at the highest pressures. The same trend is observed in the model values for plasma potential, with an error near 30% at the highest pressures. The lower temperatures at high pressures may be due to the cooling effect of electron-neutral collisions, which are not included in Eq. (22).

The model generates values for the electron density if the ionization rate  $R$  is known. The current density of primary electrons can be estimated crudely by dividing the filament emission current by the area of the vacuum chamber. The ionization rate is then  $R = n_n \sigma n_{pri} v_{pri} = n_n \sigma I_{dis} / qA$  where  $n_n$  is the neutral gas density and  $\sigma$  is the ionization cross-section. The electron density from the model using this estimate for  $R$  is shown in Fig. 9(b) along with the measured values for the density. The difference between the measured and calculated densities is small and the close agreement is probably fortuitous.

## IV. DISCUSSION

### A. Validity of the assumptions

The model is derived using several assumptions that can be checked using the experimental data. The first assumption considered is that electrons are born with negligible potential energy as a consequence of the electrostatic potential being nearly constant within the discharge. Radial potential profile measurements with the emissive probe show that the potential is indeed constant (to within 0.03 V) from the axis to a point 2 cm from the wall. The electron temperature is significantly increased if the grids covering the hot filaments are removed. The increased temperature may be a consequence of electrons being created with increased potential energy within the negative electrostatic potential perturbations near the filaments. This suggests that modeling electron energy balance in devices with unshielded filaments could be more difficult, requiring solutions for the sheath potential profile near filaments.

A second assumption is that the heating by primary electrons is negligible. This assumption is checked by calculating the heating rate from primaries using Eq. (16). The current density of primaries is estimated by dividing the chamber surface area by the filament emission current. An alternate method is to find the current density from the ionization rate calculated from Eq. (3b). These two methods give primary densities of  $\sim 1 \times 10^5 \text{ cm}^{-3}$  that is very much less than the density of wall secondaries, typically  $1.5 \times 10^6 \text{ cm}^{-3}$ . The result for the metal liners is that heating by primaries is approximately two orders of magnitude smaller than the heating by wall secondaries. This conclusion probably would not hold for plasma devices with multidipole magnetic containment that increases the primary density.

A third assumption is that the additional diffusivity in velocity space caused by the collisions of the confined electrons with the primaries and wall secondaries is small. The diffusivity in the Fokker-Planck equation, Eq. (7), is calculated using only population I electrons. The diffusivity scales with the density of field particles and inversely with the cube of their velocity. The primaries and wall secondaries have a lower density and a greater velocity than the confined electrons and thus the additional diffusivity from these electrons is negligible. The unconfined electrons are not ignored, however, when calculating the heating of the confined electrons.

A fourth assumption is that the current of primaries (population III) collected by the probe is negligible. For the 80 mA discharges, the current density of primaries estimated

from  $I_{dis}/A$  results in a probe current of  $\sim 2 \mu\text{A}$  if the distribution of primaries is isotropic. This current is comparable to the current from wall secondaries and could result in the density of wall secondaries being overestimated. However, the filaments occupy a small region of the chamber surface and the probe is oriented to minimize the cross section when viewed from the filaments. If these high-energy electrons made a significant contribution to the probe current, their contribution would be nearly constant for probe bias voltages in the range  $-6 \text{ V}$  to  $0 \text{ V}$ . The current that is observed, Fig. 5, has a slope corresponding to  $2 \text{ eV}$  for several  $e$ -foldings, and thus has the slope expected for wall secondaries rather than for primaries.

A fifth assumption is that the density of unconfined electrons from ionization (population IV) is negligible. This density may be estimated as  $Rr^*\langle 1/\nu \rangle$  by balancing the rates of creation and loss, where  $\langle 1/\nu \rangle$  is the average of the inverse velocity of population IV and  $R$  is found by using the discharge model. A typical value for  $R$  is  $4 \times 10^{17} \text{ m}^{-3} \text{ s}^{-1}$ , which gives a density of  $\sim 4 \times 10^4 \text{ cm}^{-3}$  for population IV particles. Thus they contribute negligibly to the probe current, to the Fokker-Planck diffusivity, and to the heating of confined electrons.

### B. The physical picture

The data for a discharge at  $80 \text{ mA}$  and  $0.32 \text{ mTorr}$  has been analyzed using the model to obtain the following physical picture. The ionization rate is  $R=2.7 \times 10^{17} \text{ m}^{-3} \text{ s}^{-1}$ . The mean lifetime of an ion is  $n_e/R=0.20 \text{ ms}$ . The fraction of electrons born confined is  $F(qV_p)=0.062$  and the mean lifetime of a confined electron is  $3.2 \text{ ms}$ . The secondary equilibration time is  $\tau_{se}=25 \text{ ms}$  which indicates a transfer of  $80 \text{ eV}$  per millisecond from the wall secondaries ( $T_{se} \cong 2.0 \text{ eV}$ ) to the confined electrons. This rate multiplied by  $\tau_{elec}$  yields an energy transfer of  $0.26 \text{ eV}$  per confined electron. From Eq. (21), the plasma potential should be twice the energy transferred or  $0.52 \text{ eV}$ . The measured plasma potential for these discharge conditions is  $0.56 \text{ eV}$ . The model value from simultaneous solution of the equations is  $0.78 \text{ eV}$ . The right hand side of Eq. (13) for this discharge has a value of  $5.2$  indicating that the electron temperature should be approximately  $0.19$  of the plasma potential or  $0.10 \text{ eV}$ , which is near to the measured temperature is  $0.12 \text{ eV}$ . The electron thermal velocity is  $1.9 \times 10^5 \text{ m/s}$ , which indicates that a typical electron travels  $600 \text{ m}$  before being lost. This average electron would be reflected by the sheath about  $2000$  times before being lost. The average time between collisions with neutrals is  $0.04 \text{ ms}$  which is much shorter than the time scale for heating. The short time scale for angular scattering validates the assumption that the loss boundary in velocity is spherically symmetric.

## V. CONCLUSION

A detailed discharge model based upon first principles has been developed which finds the density, temperature and plasma potential in hot-filament discharges at pressures

below  $1 \text{ mTorr}$ . The model requires as an input the density of secondary electrons from the walls that heat the confined electrons by equilibration. Experiments in a simple hot-filament discharge device show that the model gives values for density, temperature and plasma potential that are within about  $30\%$  of measured values. The experiment was not operated to find the limits to the range of parameters for which the model is accurate. However, it was demonstrated that the model is applicable only when the walls of the vacuum chamber are sufficiently clean to have a single-valued potential, which result in a single value for the energy at which electrons are lost. It was also shown that the model applies to discharges in which the filaments are covered by grids, but the model gives values for temperature that are too low for discharges with uncovered filaments.

A more useful model would be one that is in self-contained form, not requiring measured parameters as inputs. In the model, the density and temperature of the secondary electrons and the ionization rate are needed as inputs. The ionization rate is easily estimated from the discharge current, chamber area, gas pressure and ionization cross section. The secondary electron temperature is nearly always near  $2.3 \text{ eV}$  for clean metal walls. The density of wall secondaries can be estimated by the following procedure. The secondary emission coefficient  $\delta$  of the wall material can be found using the Sternglass formula for  $\delta$  with input parameters for the wall material that can be found in tables [62,63]. The current density of the secondaries at the wall is then approximately  $J_{se} = I_{dis}\delta/A$ . The secondary electron density is then found using  $J_{se} = n_{se}q\sqrt{T_{se}/2\pi m_e}$ . With this procedure, the plasma parameters may be predicted using as inputs  $\delta$ ,  $I_{dis}$ , the chamber volume and area, the gas pressure, and the ionization cross section [62].

It is likely that the model can be extended to other types of discharges, for example, hot-filament discharges with surface magnetic containment that give much higher densities of confined electrons. This application will require a more detailed model for the heating by the primaries that includes their spread in energy caused by their losing energy to ionization. In addition, the effective areas for the losses of electrons and ions are likely to be different from one another and different from the area of the chamber walls. The model might also be extended to cold-cathode discharges. The electrons from these cathodes pass through discharges at low pressure without slowing sufficiently to be trapped, thus the heating of the confined electrons is by equilibration with the primaries and wall secondaries. These discharges operate at higher pressures, so the model for ion losses should be based upon ion mobility rather than the "free fall" model. The experiments show that accurate modeling of energy balance is likely to be very difficult for any device not having a constant wall potential.

## ACKNOWLEDGMENTS

The authors thank Dr. Arthur V. Phelps for many useful discussions and thank Scott Knappmiller for numerous modifications to the experiment and for data acquisition.

- [1] A. Lang and N. Hershkowitz, *J. Appl. Phys.* **49**, 4707 (1978).
- [2] M.-H. Cho, N. Hershkowitz, and T. Intrator, *J. Appl. Phys.* **67**, 3254 (1990).
- [3] N. Hershkowitz, R. L. Goettsch, C. Chan, K. Hendricks, and R. T. Carpenter, *J. Appl. Phys.* **53**, 5330 (1982).
- [4] N. Hershkowitz and K. N. Leung, *Appl. Phys. Lett.* **26**, 607 (1975).
- [5] A. J. T. Holmes, *Rev. Sci. Instrum.* **52**, 1814 (1981).
- [6] A. P. H. Goede and T. S. Green, *Phys. Fluids* **25**, 1797 (1982).
- [7] A. Smirnov, Y. Raitses, and N. J. Fisch, *J. Appl. Phys.* **94**, 852 (2003).
- [8] R. J. Taylor, K. R. MacKenzie, and H. Ikezi, *Rev. Sci. Instrum.* **43**, 1675 (1972).
- [9] E. R. Ault and K. R. MacKenzie, *Rev. Sci. Instrum.* **44**, 1697 (1973).
- [10] R. Limpacher and K. R. MacKenzie, *Rev. Sci. Instrum.* **44**, 726 (1973).
- [11] I. Langmuir, *Phys. Rev.* **26**, 585 (1925).
- [12] L. D. Tsendin and Yu. B. Golubovskii, *Zh. Tekh. Fiz.* **47**, 1839 (1977) [*Sov. Phys. Tech. Phys.* **22**, 1066 (1977)].
- [13] D. Bohm, in *The Characteristics of Electrical Discharges in Magnetic Fields*, edited by A. Guthrie and R. Wakerling (McGraw-Hill, New York, 1949), Chap. 3.
- [14] L. Tonks and I. Langmuir, *Phys. Rev.* **34**, 876 (1929).
- [15] E. R. Harrison and W. B. Thompson, *Proc. Phys. Soc. London* **74**, 145 (1959).
- [16] J. R. Forrest and R. N. Franklin, *J. Phys. D* **1**, 1357 (1968).
- [17] R. N. Franklin, *Plasma Phenomena in Gas Discharges* (Clarendon, Oxford, 1976), Chap. 2.6.
- [18] H. Brunet and P. Vincent, *J. Appl. Phys.* **50**, 4700 (1979).
- [19] A. Maresca, K. Orlov, and U. Kortshagen, *Phys. Rev. E* **65**, 056405 (2002).
- [20] M. N. Rosenbluth, W. M. MacDonald, and D. L. Judd, *Phys. Rev.* **107**, 1 (1957).
- [21] W. M. MacDonald, M. N. Rosenbluth, and W. Chuck, *Phys. Rev.* **107**, 350 (1957).
- [22] V. P. Pastukhov, *Nucl. Fusion* **14**, 3 (1974).
- [23] D. P. Chernin and M. N. Rosenbluth, *Nucl. Fusion* **18**, 47 (1978).
- [24] R. H. Cohen, M. E. Rensink, T. A. Cutler, and A. A. Mirin, *Nucl. Fusion* **18**, 1229 (1978).
- [25] J. H. Ingold, *Phys. Rev. E* **56**, 5932 (1997).
- [26] L. D. Tsendin, *Plasma Sources Sci. Technol.* **4**, 200 (1995).
- [27] V. I. Kolobov and V. A. Godyak, *IEEE Trans. Plasma Sci.* **23**, 503 (1995).
- [28] M. A. Biondi, *Phys. Rev.* **93**, 1136 (1954).
- [29] V. S. Egorov, Yu. B. Golubovskii, E. Kindel, I. B. Mekhov, and C. Schimke, *Phys. Rev. E* **60**, 5971 (1999).
- [30] A. V. Phelps and L. C. Pitchford, *Phys. Rev. A* **31**, 2932 (1985).
- [31] M. J. Hartig and M. J. Kushner, *J. Appl. Phys.* **73**, 1080 (1993).
- [32] C. Busch and U. Kortshagen, *Phys. Rev. E* **51**, 280 (1995).
- [33] D. Uhrlandt and R. Winkler, *J. Phys. D* **29**, 115 (1996).
- [34] U. Kortshagen, G. J. Parker, and J. E. Lawler, *Phys. Rev. E* **54**, 6746 (1996).
- [35] U. Kortshagen, C. Busch, and L. D. Tsendin, *Plasma Sources Sci. Technol.* **5**, 1 (1996).
- [36] E. A. Richley, *Phys. Rev. E* **66**, 026402 (2002).
- [37] R. R. Arslanbekov and A. A. Kudryavtsev, *Phys. Plasmas* **6**, 1003 (1999).
- [38] R. R. Arslanbekov, A. A. Kudryavtsev, and L. D. Tsendin, *Phys. Rev. E* **64**, 016401 (2001).
- [39] U. Kortshagen and J. Schlüter, *J. Phys. D* **25**, 644 (1992).
- [40] P. A. Sá, J. Loureiro, and C. M. Ferreira, *J. Phys. D* **25**, 960 (1992).
- [41] L. D. Tsendin, *Plasma Sources Sci. Technol.* **4**, 200 (1995).
- [42] G. G. Lister, *J. Phys. D* **25**, 1649 (1992).
- [43] S. A. Self, *J. Appl. Phys.* **36**, 456 (1965).
- [44] S. A. Self and H. N. Ewald, *Phys. Fluids* **9**, 2486 (1966).
- [45] Z. Sternovsky, *Plasma Sources Sci. Technol.* **14**, 32 (2005).
- [46] C. B. Opal, W. K. Peterson, and E. C. Beaty, *J. Chem. Phys.* **55**, 4100 (1971).
- [47] J. T. Grissom, R. N. Compton, and W. R. Garrett, *Phys. Rev. A* **6**, 977 (1972).
- [48] S. Yoshida, A. V. Phelps, and L. C. Pitchford, *Phys. Rev. A* **27**, 2858 (1983).
- [49] I. P. Shkarofsky, T. W. Johnston, and M. P. Bachynski, *The Particle Kinetics of Plasmas* (Addison-Wesley, Reading, MA, 1966), Eqs. 7-71, 7-87 and 7-134.
- [50] R. Kollath, *Ann. Phys.* **6**, 357 (1947).
- [51] G. A. Harrower, *Phys. Rev.* **104**, 52 (1956).
- [52] D. Diebold, N. Hershkowitz, A. D. Bailey III, M. H. Cho, and T. Intrator, *Rev. Sci. Instrum.* **59**, 270 (1988).
- [53] Z. Sternovsky and S. Robertson, *Phys. Plasmas* **11**, 3610 (2004).
- [54] S. Robertson, Z. Sternovsky, and B. Walch, *Phys. Plasmas* **11**, 1753 (2004).
- [55] H. Mott-Smith, Jr. and I. Langmuir, *Phys. Rev.* **28**, 727 (1926).
- [56] F. F. Chen, in *Plasma Diagnostic Techniques*, edited by R. H. Huddlestone and S. L. Leonard (Academic, New York, 1965), Chap. 4.
- [57] M. J. Goeckner, J. Goree, and T. E. Sheridan, *Phys. Fluids B* **3**, 2913 (1991).
- [58] G. Bachet, L. Chérigier, M. Carrère, and F. Doveil, *Phys. Fluids B* **5**, 3097 (1993).
- [59] Z. Sternovsky and S. Robertson, *Appl. Phys. Lett.* **81**, 1961 (2002).
- [60] Z. Sternovsky, S. Robertson, and M. Lampe, *Phys. Plasmas* **10**, 300 (2003).
- [61] Z. Sternovsky, S. Robertson, and M. Lampe, *J. Appl. Phys.* **94**, 1374 (2003).
- [62] E. J. Sternglass, *Phys. Rev.* **80**, 925 (1950).
- [63] D. J. Gibbons, in *Handbook of Vacuum Physics*, edited by A. H. Beck (Pergamon, Oxford, 1964), Vol. 2, p. 301.